Study of the gelation kinetics during molecularly imprinted membrane formation

Yun Ying Zhai, Pin Zhang, Yanbin Yun*, Jingjing Liu, Zejun Huang, Qiang Xia

School of Environmental Science and Engineering, Beijing Forestry University, Beijing, 100083, China,
email: 438583570@qq.com (Y.Y. Zhai), 1183581868@qq.com (P. Zhang), yunyanbin@bjfu.edu.cn (Y. Yun),
83222480@qq.com (J. Liu), 502777401@qq.com (Z. Huang), 1262786601@qq.com (Q. Xia)

ABSTRACT

Molecularly imprinted membranes have been researched for many years, however, little attention has been focused on the gelation kinetics during these membranes' formation. In this paper, three kinds of molecularly imprinted membranes were prepared through the phase inversion method by adding kaempferol as template molecule and imprinted polymer sphere and blank, respectively, the gelation kinetic processes were investigated in detail. It was found that the average gelation velocities of the skin layer ($\bar{v}_1$) > the average gelation velocities of the transition layer ($\bar{v}_2$) > the average gelation velocities of the support layer ($\bar{v}_3$) for the blank membrane, kaempferol molecularly imprinted membranes and polymer sphere molecularly imprinted membranes. The average gelation velocity of the molecularly imprinted membranes was faster than that of the blank membrane during the whole membrane formation process. Furthermore, the casting solution (formulation and viscosity), the gelation velocity and the membrane performances (water flux and rejection) were relative according to the experimental data analysis. All membranes prepared in this study exhibited asymmetric finger- like structures. In addition, three kinds of membranes were respectively tested their adsorption properties.

Keywords: Molecular imprinting; Membrane; Kaempferol; Polymer sphere; Gelation velocity

1. Introduction

Molecular imprinting technology, which has been applied widely in biosensor, separation, and catalysis nowadays, developed rapidly and obtained a lot of attention. Since the 21st century, many research institutions have focused on molecularly imprinted membrane (MIM) technology, which combines membrane separation and molecular imprinting technology [1]. Inheriting the advantages of both, MIM are characterized by selective recognition, high binding capacity and excellent permeability [2–4], which can be applied widely for novel separation device, chemical sensor with high stability and selectivity, and drug delivery system [3,5].

The application of this technique to produce hybrid systems based on the dispersion of cross-linked imprinted polymers into commonly used polymer matrices, had great influence on the separation performance [6,7] of these systems. This approach, which was known as "hybrid molecular imprinting", had been described in some papers [8] dealing with the preparation of hybrid polymeric membranes for application in clinical field [9,10] and enantioseparation [11].

During the membrane formation process, both kinetic effect and thermodynamic effect determined the membrane structure which has a dense skin layer, a medium dense transition layer and a loose finger-like support layer, the pore size and distribution are mainly controlled by kinetic effects [12]. Many researchers attempted to explain the membrane formation mechanism with the help of gelation kinetics, thus membrane performances can be controlled [12,13]. The ternary phase diagram for a polymer-solvent-nonsolvent system and the relation between X^2 (X represented the gelation front movement distance) and the gelation time t were usually used to investigate the gelation kinetics [3,13–16]. However, they had not studied the change of the velocity

*Corresponding author.

during the gelation process through the relationship of v and t, which can affect the membrane performance and structure directly. In addition, most of the studies were just for ultra filtration membranes.

Through literature search [1], it was found that sulfone and hydroxyl groups can form hydrogen bonds, and thus the synthesized MIM has excellent separation performance for kaempferol. In the paper, two molecularly imprinted membranes were prepared by phase inversion method and adding kaempferol and kaempferol molecularly imprinted polymer spheres, respectively. In addition, polyacrylonitrile (PAN) was used as the membrane material because of its chemical stability, hydrophilicity and good solubility [17,18]. For molecularly imprinted membranes, the gelation velocity was put forward to research the gelation kinetics, which was calculated through the relationship between X and t during the molecularly imprinted membranes gelation process.

2. Materials and method

2.1. Materials

PAN was supported by Beijing Hongzhijiahe Technology Co., Ltd., Beijing, China. N, N-dimethylformamide (DMF) as solvent was obtained from Beijing Chemical Works, Beijing, China. Polyethylene oxide-poly propylene oxide-polyethylene oxide (PEO-PPO-PEO) and $Mg(ClO_4)_2$ selected as additives were purchased from Beijing Ansimosen Technology Co., Ltd., Beijing, China and Tianjin Jinke Fine Chemical Institute, Tianjin, China, respectively. Bull serum albumin (BSA, Mw 67,000 Da) was purchased from Sinopharm Chemical Reagent Beijing Co., Ltd., Beijing, China. Kaempferol (Mw 286 Da, specification 98%) and rutin were obtained from Xi'an Tonking Biotech Co., Ltd, Shanxi, China and the Kaempferol molecular structural formula is shown in Fig. 1. Nano-TiO$_2$ was purchased from Jiangsu Hohai Nano Technology Co., Ltd. Ethylene glycol dimethacrylate (EDMA) was purchased from Alfa Aesar, EDMA was purified by reduced pressure distillation to remove inhibitor before polymerization. Methacrylate(MAA) and 2,2-azobisisobutyronitrile (AIBN) were purchased Tianjin Jinke fine chemical institute, Tianjin, China. Toluene was analytical grade and purchased from Beijing Chemical works, Beijing, China.

2.2. Synthesis of imprinted polymer micro spheres

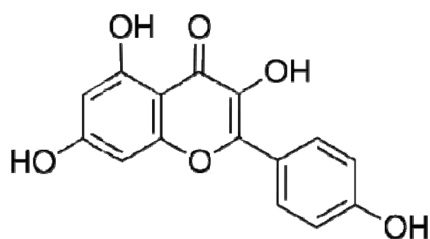Kaempferol molecularly imprinted polymer (MIP) micro sphere was prepared by surface molecular imprinting technology using EDMA as cross-linker and MAA as the functional monomer in toluene. The template molecule kaempferol and MAA were dissolved in toluene in a conical flask until well mixed and nano-TiO$_2$ was added at room temperature and stirred continuously. Then, EDMA and AIBN were added to the above mixed solution, and the solution was degassed in an ultrasonic bath and sprayed with oxygen-free nitrogen. The resulting polymer was cooled to room temperature and collected by centrifugation [20]. Non-imprinted polymer (NIP) micro spheres were also prepared in identical manner but without the addition of kaempferol.

2.3. Preparation of molecularly imprinted membranes

The molecularly imprinted membranes were prepared by the phase inversion method. Firstly PAN, additives $(Mg(ClO_4)_2$, PEO-PPO-PEO), template kaempferol (The mass concentration range is 0 wt.% to 2.5 wt.%.) and imprinted polymer spheres (The mass concentration range is 0 wt.% to 0.5 wt.%.) were dissolved in DMF (Table 1) at 40°C separately stirred for 24 h to ensure the homogeneous mixing. The solution is allowed to stand for 24 h so that the bubbles are completely released. Then the solution was casted on the flat glass by using a casting knife, and immersed in a non solvent coagulation bath (pure water) until solidified. In order to remove all the residual solvent, the membranes were moved into another pure water bath and kept at room temperature for 12 h.

In addition, to use MIP or NIP instead of kaempferol, the MIPM and NIPM were respectively prepared in the same way.

2.4. Kinetic experiments

The gelation velocity of both imprinted and blank membranes was investigated. The gelation process of the molecularly imprinted membrane formation was observed by using an online optical microscope-camera experimental system which contains an OPTEC BDS200-PH optical inverted microscope, a USB2.0 camera, a 1/2"CMOS color image sensor, a computer and two specially designed microscope slides. By using this system, images of 30 frames per second can be obtained and the magnification could be changed from 40× to 1200×. During the test, a drop of the casting solution was placed between the two special microscope slides. Then a drop of pure water, which was used as the precipitant, was carefully injected into one of the holes on the upper slide by a syringe. Images were automatically captured by the camera as soon as the pure water started to contact with the casting solution. The velocity (v) was calculated by:

$$V = \frac{dX}{dt} \tag{1}$$

where X represents the gelation front movement distance and t is the time.

2.5. Experiments of viscosity, water flux and BSA rejection

The viscosity of the prepared casting solution was measured using a rotational viscometer (NDJ-1, Shanghai Changji Co., Ltd., Shanghai, China) at room temperature.

Fig. 1. Molecular structural formula of kaempferol.

Table 1
Formulations of different casting solutions

	PAN (wt. %)	$Mg(ClO_4)_2$ (wt. %)	PEO-PPO-PEO (wt. %)	Kaempferol (wt. %)	Imprinted polymer spheres (wt. %)
Blank membrane	10.0	1.0	1.5	0	0
Kaempferol molecularly imprinted membrane	10.0	1.0	1.5	0.5	0
				1.0	0
				1.5	0
				2.0	0
				2.5	0
Polymer sphere molecularly imprinted membrane	10.0	1.0	1.5	0	0.1
				0	0.2
				0	0.3
				0	0.4
				0	0.5

Membranes were characterized in terms of water flux and BSA rejection, which were both measured with a cross-flow system under 0.10 MPa and at 25°C. The pure water was used to determine the water flux (Flux), which is calculated according to:

$$Flux = \frac{Q}{At} \qquad (2)$$

where Q is the volume of the permeate pure water (L); A denotes the effective area of the membrane (m²); t represents the filtration time (h). The rejection was measured using 500 mg/L BSA solution, then the BSA concentrations in the feed and permeated were determined separately using a UV-spectrophotometer (UNICO-UV2102, China) at the wavelength of 280 nm and Rejection of BSA is expressed by:

$$Rejection = \left(\frac{1 - C_p}{C_f} \right) \times 100 \ \% \qquad (3)$$

where C_p and C_f are respectively the concentrations of the permeation and the feed. At least three sets of the membrane samples were tested for each condition and the average value was reported.

2.6. Morphology of molecularly imprinted membranes

The membrane morphology was observed with scanning electron microscopy (SEM, Quanta 200, FEI Co., Ltd, Holland). For determining the membrane cross-section, membrane samples were firstly immersed in liquid nitrogen and fractured quickly using tweezers. Since the sample is nonconducting, metallic gold was sputter on the membrane surface by a sputter gun. Finally, the golden coated samples were observed.

2.7. Adsorption and selectivity experiments

Cut pieces of the membranes and 40.0 mL kaempferol ethanol solution were put in conical flasks and shaken for 24 h at 50°C in a shaking table. The temperature that the reference used is 50°C [1]. At the adsorption kinetics experiment, the 10 mg/l kaempferol were shaken from 0 to 500 s. In the adsorption isotherm part, the adsorption time was 300 s, the conical flasks that contained 1 to 20 mg/l kaempferol were shaken. After that the solution was measured by UV-spectrophotometer. Absorptiometry was used to determine kaempferol concentration, and the wavelength was 370 nm.

Rutin was selected as an interfering substance to evaluate the selectivity of MIM to kaempferol. The kaempferol and rutin mix solution was used to evaluate the selectivity of the MIMs to kaempferol. One piece of MIM was put in 10.0 mL kaempferol-rutin mix ethanol solution, after that it was transferred in conical flasks and shaken for 24 h at 30°C in a shaking table. The selected 30°C was the room temperature at the time that the experiment took place. Ultraviolet and visible spectrophotometer was used to determine kaempferol and rutin concentration, and the wavelength were 370 and 270 nm, respectively [2].

$$K_D = \frac{C_p}{C_e} \qquad (4)$$

$$\alpha = \frac{K_{Di}}{K_{Dj}} \qquad (5)$$

where C_p and C_e were the adsorption quantity of the substrate and the equilibrium adsorption, respectively; K_{Di} and K_{Dj} were the binding site balance dissociation constant for template molecule and interference molecule; and α was separation factor.

3. Results and discussion

3.1. Gelation velocity of the blank membrane

The relationship between the gelation velocity and the time is shown in Fig. 2a, it was found that the velocity decreased gradually as the gelation time went on. As the asymmetric membrane contained the skin layer, the transition layer and the support layer, Qin et al. [4,17] found that the skin layer formation was finished within the first 0.5 s,
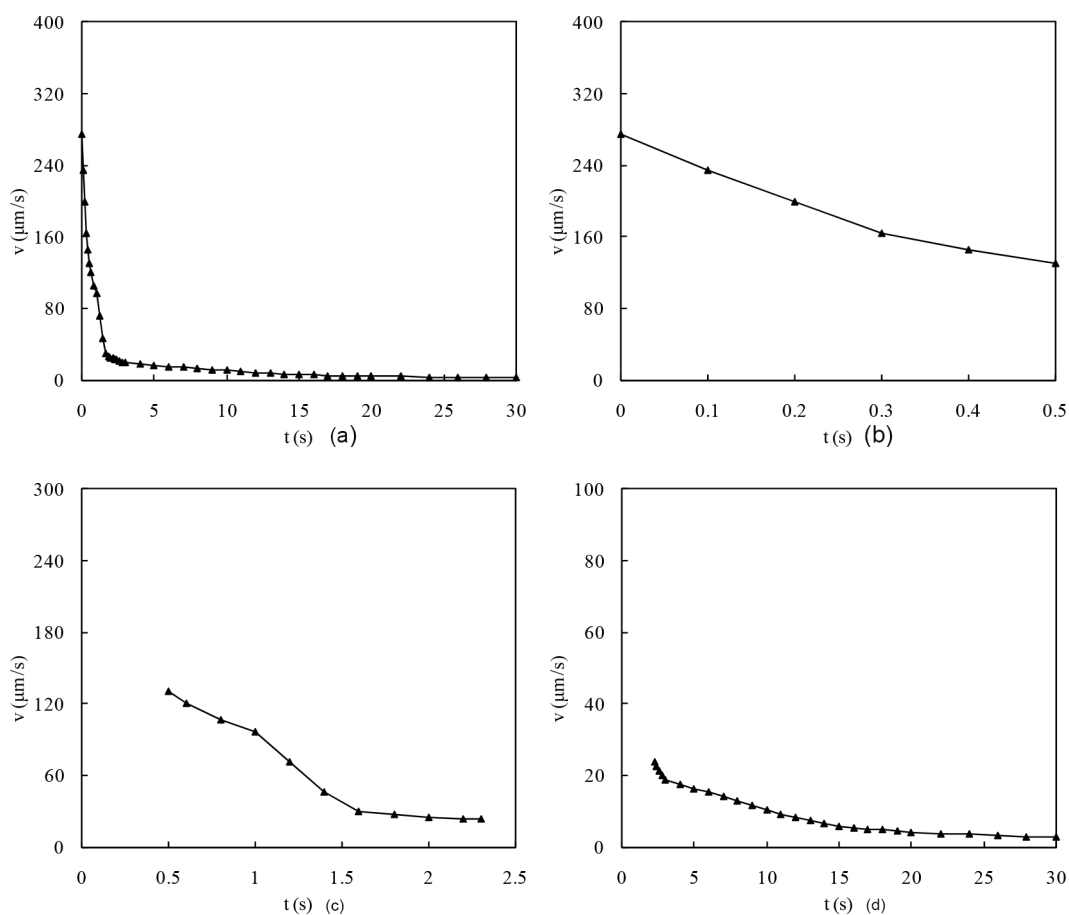
Fig. 2. The relationship between the gelation velocity and the time for the blank membrane. (a), (b), (c), (d) represent 0–30 s, 0–0.5 s, 0.5–2.3 s and 2.3–30 s, respectively.

the transition layer formation was finished at 2.3 s and the remaining time was for the support layer formation. Thus the gelation process shown in Fig. 2a can be divided into three different processes (b, c, d). The initial mass transfer velocity between solvent and non solvent was very fast, thus the gelation velocity was the highest at first (b). Then the transfer resistance between casting solution and coagulation bath increased due to the formation of the skin layer, so the gelation velocity decreased (c). The gelation velocity of the support layer was the lowest because the skin layer and the transition layer formed (d). The gelation velocity of the skin layer controls the structure, the pore size and the pore number of the membrane which affect the membrane performances, hence it is significant to investigate the velocity of the skin layer formation. For the blank membrane, the casting solution viscosity was 3016.0 MPa·s, the water flux and rejection were 3846.2 L/m²h and 82.3%, respectively.

3.2 Effects of kaempferol concentration on gelation velocity for molecularly imprinted membranes

As the gelation velocity continuously decreased during the membrane formation, the gelation velocities of the skin layer, the transition layer and the support layer cannot be

compared with quantitatively, furthermore, it is also hard to compare with the gelation velocities of different membrane quantitatively. So, the average gelation velocity is presented for the quantitative investigation rather than the qualitative analysis, which is calculated by:

$$\overline{v} = \frac{\left(\sum (i=1)^n v_i \right)}{n} \tag{6}$$

where n is the number of calculative velocity during the special time of the membrane formation, $\overline{v}_1$, $\overline{v}_2$ and $\overline{v}_3$ represent the average gelation velocity of skin layer, transition layer and support layer, respectively.

For the blank membrane, $\overline{v}_1$, $\overline{v}_2$ and $\overline{v}_3$ was 191, 63 and 10 μm/s, respectively, for the kaempferol molecularly imprinted membranes, it also can be found that $\overline{v}_1 > \overline{v}_2 > \overline{v}_3$ (Table 2). As the gelation velocity of the skin layer controls the membrane properties, $\overline{v}_1$ is the most important compared with $\overline{v}_2$ and $\overline{v}_3$, so $\overline{v}_1$ is focused to discuss in the following discussions.

As the kaempferol concentration went up from 0 to 0.5 wt. %, the decreasing casting solution viscosity (Fig. 3) caused a shorter gelation process, $\overline{v}_1$ increased from 191 to 298 μm/s (Fig. 4, Table 2), which caused larger membrane pores while the pore number was less, hence the rejection and the water flux declined from 82.3 to 81.6 %

Table 2
Effects of the kaempferol concentration on the average gelation velocity

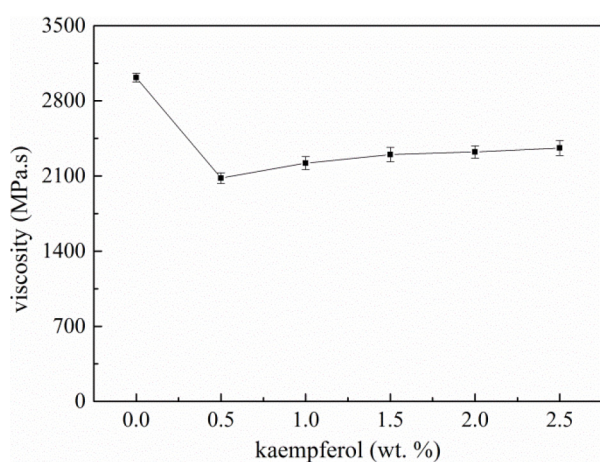| Kaempferol concentration (wt. %)	$\bar{v}_1$ (µm/s)	$\bar{v}_2$ (µm/s)	$\bar{v}_3$ (µm/s)
0	191	63	10
0.5	298	125	24
1.0	276	112	20
1.5	223	91	19
2.0	209	100	21
2.5	221	99	22

Fig. 3. Effects of kaempferol concentration on casting solution viscosity.

and 3846.2 to 2217.5 L/m² h (Fig. 5), respectively. When the kaempferol concentration further rose from 0.5 to 1.5 wt. %, the enlarged casting solution viscosity (from 2080.0 to 2300.0 MPa·s) limited the movement of macromolecular segment, the diffusion of precipitation into casting solution became slower [17], thus the phase separation time delayed and the gelation velocity declined from 298 to 223 µm/s, however, the kaempferol micelles formed which induced the formation of some macrovoids, as a result, the water flux ascended from 2217.5 to 2778.1 L/m² h while the rejection declined from 81.6 to 64.0 %. With an increasing kaempferol concentration from 1.5 to 2.0 wt. %, the casting solution viscosity increased from 2300.0 to 2324.0 MPa·s, thus $\bar{v}_1$ declined from 223 to 209 µm/s, the membrane should have thicker skin layer, hence the water flux decreased from 2778.1 to 2450.6 L/m² h, meanwhile, some macrovoids were formed because of the formation of kaempferol micelles, thus the rejection dropped from 64.0 to 51.0%. With the increase of kaempferol concentration ranged from 2.0 to 2.5 wt. %, more hydrogen bonds form between kaempferol and DMF weakened the solvent activity and the thermodynamic stability of casting solution, $\bar{v}_1$ increased from 209 to 221 µm/s mildly, which could cause some large pores, meanwhile, the further enlarged casting solution viscosity (Fig. 3) led to a denser skin layer, thus the water flux decreased from 2450.6 to 2277.3 L/m²h and

the rejection declined from 51.0 to 28.3%. Fig. 6 reveals that with the kaempferol concentration increasing, the finger-like structure of membranes became more and more irregular.

3.3. Effects of imprinted polymer sphere concentration on gelation velocity for molecularly imprinted membranes

As shown in Fig. 8 and Table 3, with an increasing imprinted polymer sphere concentration from 0 to 0.1 wt. %, the declined casting solution viscosity caused $\bar{v}_1$ increasing from 191 to 193 µm/s, thus some large pores could form. Furthermore, nano-TiO$_2$ of the imprinted polymer sphere could not only enhance the membrane's porosity, but also attracted water molecules inside the membrane matrix and promote them to pass through membrane [23]. As a result, the rejection of BSA declined from 82.3 to 71.9% and the water flux increased from 3846.2 to 4198.3 L/m²h (Fig. 9). As the imprinted polymer sphere concentration rose from 0.1 to 0.2 wt. %, the casting solution viscosity was enlarged from 2440.0 to 2464.0 MPa·s, which should result in a dense skin layer. However, the weakened casting solution thermodynamic stability which owing to the hydrogen bonds formed between imprinted polymer spheres and DMF increased $\bar{v}_1$ from 193 to 290 µm/s, the two impacts offset each other, thus the pore number and pore size changed slightly, thus the water flux and rejection kept basically stable at 4150.0 L/m² h and 82.0%, respectively. As the imprinted polymer sphere concentration went up from 0.2 to 0.3 wt. %, the enlarged casting solution viscosity (Fig. 7) decreased $\bar{v}_1$ from 290 to 210 µm/s, thus the skin layer of membrane became denser, meanwhile there were some macrovoids caused by aggregate imprinted polymer spheres, the water flux and the rejection declined from 4116.0 to 3461.5 L/m² h and 81.6 to 74.8% respectively. When the imprinted polymer sphere concentration ranged from 0.3 to 0.5 wt. %, the casting solution viscosity rose from 2680.0 to 2964.0 MPa·s. However, more hydrogen bonds between imprinted polymer spheres and DMF could weaken the DMF activity and the thermodynamic stability of the casting solution, $\bar{v}_1$ went up from 210 to 256 µm/s. Because of the two impacts which offset each other, the water flux changed mildly between 3440.0 and 3534.0 L/m² h, the aggregate imprinted polymer spheres made some large pore, hence the rejection decreased from 72.0 to 67.0%. SEM micrographs shown in Fig. 10 display that the pore wall of the finger-like structure became looser than the membranes with kaempferol.

Compared with the average gelation velocities of different membranes through Tables 2 and 3, it can be found that for the membranes prepared in this study $\bar{v}_1 > \bar{v}_2 > \bar{v}_3$, meanwhile, the increasing concentrations of kaempferol and imprinted polymer sphere had different effects on the gelation kinetic process. The increasing concentrations of kaempferol (0.5 to 2.5 wt. %) and imprinted polymer sphere (0.1 to 0.5 wt. %) resulted in $\bar{v}_1$ fluctuating between 209 and 298 µm/s, 193 and 290 µm/s respectively, $\bar{v}_2$ and $\bar{v}_3$ with kaempferol were faster than those with imprinted polymer spheres. When the kaempferol and imprinted polymer sphere concentrations were both 0.5 wt. %, $\bar{v}_1$, $\bar{v}_2$ and $\bar{v}_3$ with imprinted polymer sphere were slower, which could be due to a higher casting solution viscosity.
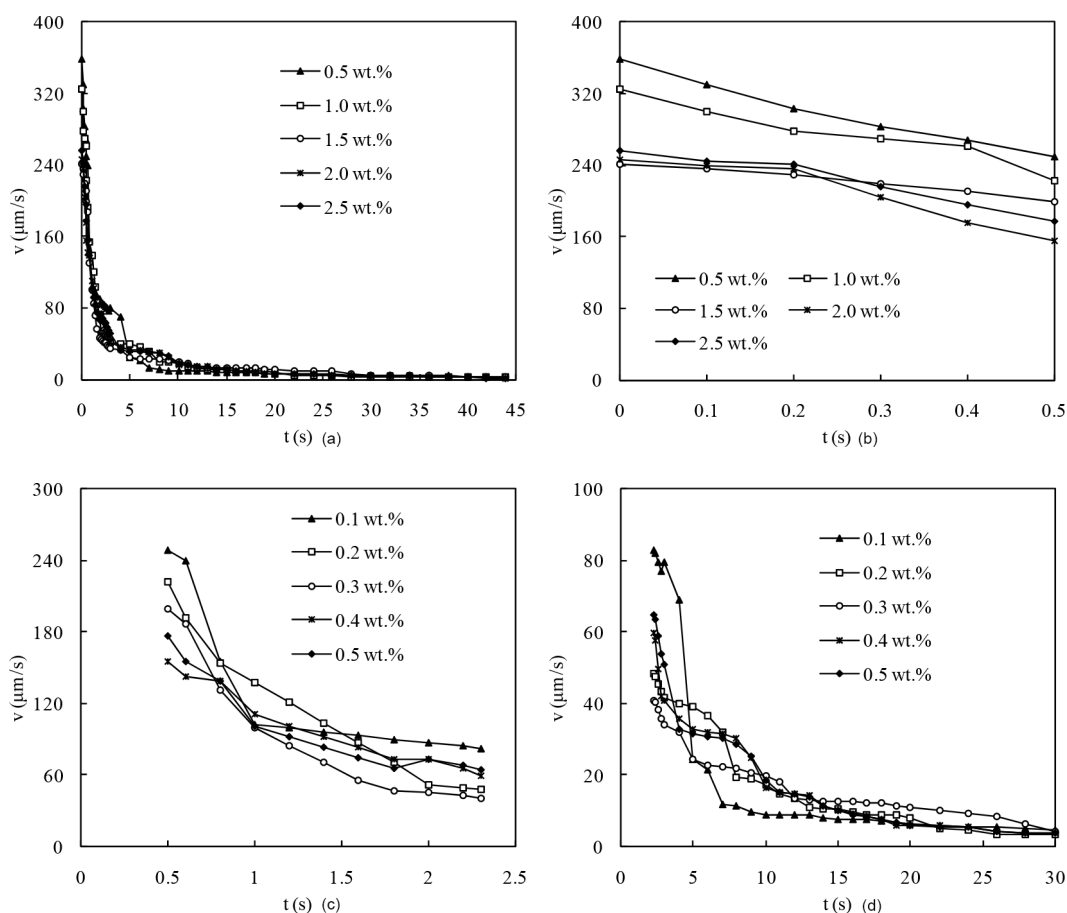
Fig. 4 Effects of kaempferol concentration on the relationship between the gelation velocity and the time for kaempferol molecularly imprinted membranes. (a), (b), (c), (d) represent 0–30 s, 0–0.5 s, 0.5–2.3 s and 2.3–30 s, respectively.
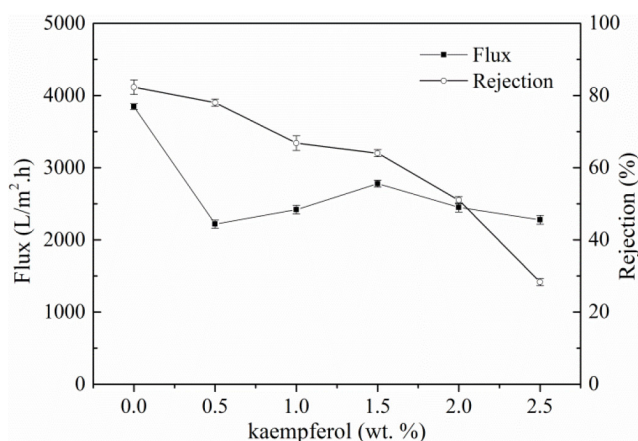

Fig. 5 Effects of kaempferol concentration on flux and rejection.

3.4. Adsorption experiments and selectivity experiments

Adsorption kinetics and adsorption isotherms were obtained for the adsorption of kaempferol. From the adsorption kinetic curve Fig. 11a, it is shown that as the adsorption prolonged, the adsorption amount increased slowly, and the adsorption amount of MIM reached 450 µg/g at 400 s. It is shown in the adsorption kinetic curve that as the adsorption prolonged, the adsorption amount of MIM slowly increased and reached 450 µg/g at 400 s; in contrast, the amount of MIPM was 340 µg/g, which was a little bit lower than the amount of MIM. The amount of NIM had also showed its scarcity towards kaempferol, which was 120 µg/g.

From the adsorption isotherm curve Fig. 11b, the adsorption quantity quickly rose as the kaempferol solution increased before the 2.5 wt. % kaempferol ethanol solution; the max adsorption quantity also was MIM, and it was 248 µg/g and the adsorption quantity of MIPM reached 166 µg/g. NIPM and NIM were similar, which were 62.1 and 55.8 µg/g, respectively. From this we can know that MIM can achieve the maximum adsorption capacity. Although the high adsorption capacity of MIPM for kaempferol is due to the presence of MIP, as the amount of MIP is not enough, so the adsorption capacity of MIPM cannot reach the maximum. In the early stage of MIM, kaempferol is easily adsorbed. When the surface binding sites become full, adsorption of internal binding sites will be started. However, the surface adsorbent may hinder the movement of molecules to the inside, so the adsorption rate becomes slower.
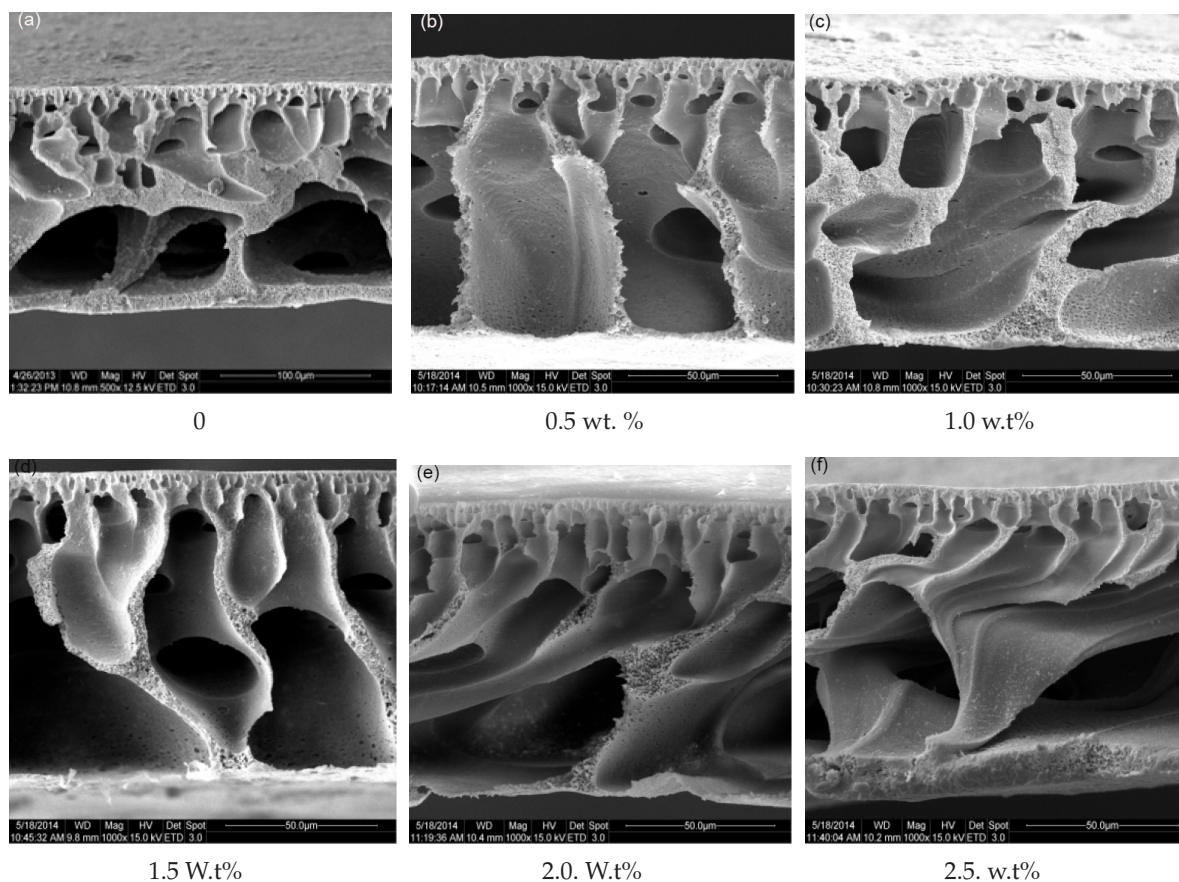
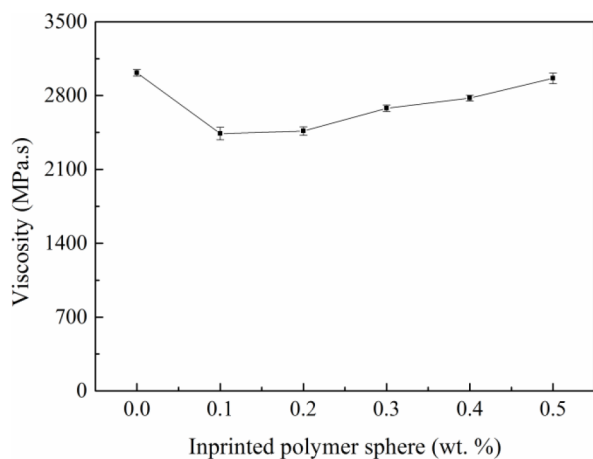Fig. 6. Cross-sectional SEM micro graphs of membranes for different kaempferol concentrations.

Fig. 7. Effects of imprinted polymer sphere concentration on casting solution viscosity

Separation factor (α) was an important factor to evaluate the selectivity of MIM, MIPM, NIPM, NIM. It can be calculated by the equilibrium dissociation constant (K_D). Table 4 shows the equilibrium dissociation constant (K_D) of MIM, MIPM, NIPM and NIM to kaempferol and rutin respectively, as well as the calculated separation factors (α). Obviously, in the presence of competitor rutin, MIM still has a higher specific adsorption for kaempferol, with a separation factor of 3.75. Although the molecular structure of rutin is similar to that of kaempferol, MIM still has a high specific selectivity. The separation factor of MIPM was slightly lower than 3.45 for MIM, but the specificity of selection was better. The separation factors for NIPM and NIM were 1.13 and 0.95, respectively. When the separation factor is greater than 1, this means that kaempferol can be effectively separated under interference conditions. After comprehensive comparison, the specificity of MIM for kaempferol is best.

4. Conclusions

In this paper, the gelation rates of blank and molecularly imprinted membranes in kaempferol solution were investigated. It was found that the gelation rate of the surface layer controls the membrane structure, pore size, and number of pores that affect the membrane properties. Therefore, the surface layer was studied. The speed of formation was crucial. Comparing blank and molecularly imprinted membranes, we found that $\bar{v}_1 > \bar{v}_2 > \bar{v}_3$. With the increase of the concentration of kaempferol or imprinted polymer spheres, the viscosity of the casting solution decreased and then increased. The rejection of BSA significantly decreased, and the inhibitory effect of
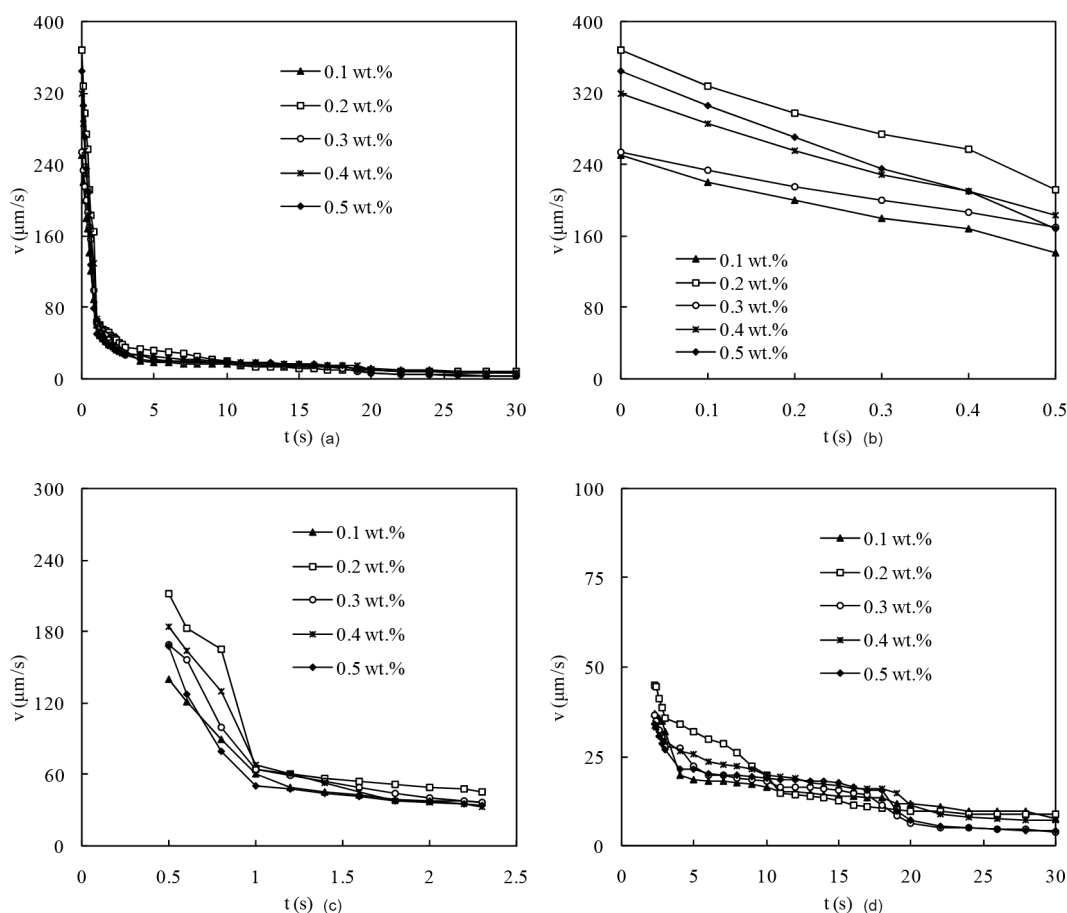
Fig. 8. Effects of imprinted polymer sphere concentration on the relationship between the gelation velocity and the time for polymer sphere molecularly imprinted membranes. (a), (b), (c), (d) represent 0 to 30 s, 0 to 0.5 s, 0.5 to 2.3 s and 2.3 to 30 s, respectively.

Table 3
Effects of the imprinted polymer sphere concentration on the average gelation velocity

Imprinted polymer sphere concentration (wt. %)	$\bar{v}_1$ (µm/s)	$\bar{v}_2$ (µm/s)	$\bar{v}_3$ (µm/s)
0	191	63	10
0.1	193	64	18
0.2	290	90	21
0.3	210	73	17
0.4	247	77	19
0.5	256	64	17

Fig. 9 Effects of imprinted polymer sphere concentration on flux and rejection.

kaempferol on the membrane was significantly weakened. The MIM with the best adsorption effect was 400 s in equilibrium and the maximum adsorption capacity was 450 µg/g in a 20 mg/l ethanol solution of kaempferol. At the same time, the separation of MIM in the mixed solution of rutin and kaempferol was the most effective and the separation factor was 3.75. Comprehensive evaluation, MIM has a better selective adsorption capacity.
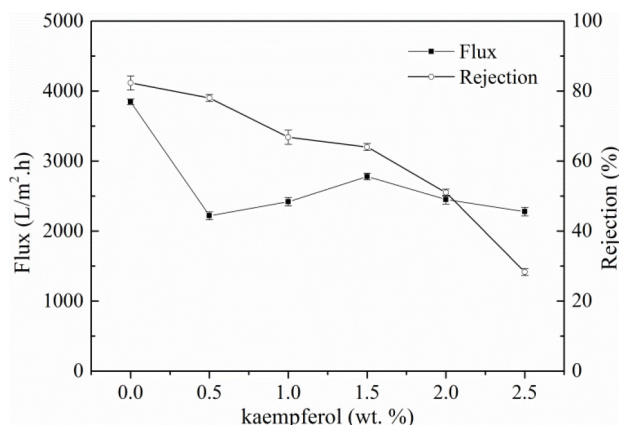
In addition, the initial experiment of adding PAN in the basic experiment, the interaction between PAN and kaempferol is a hypothesis of hydrogen bonds and physical effects, so this will become a research direction in future experiments.
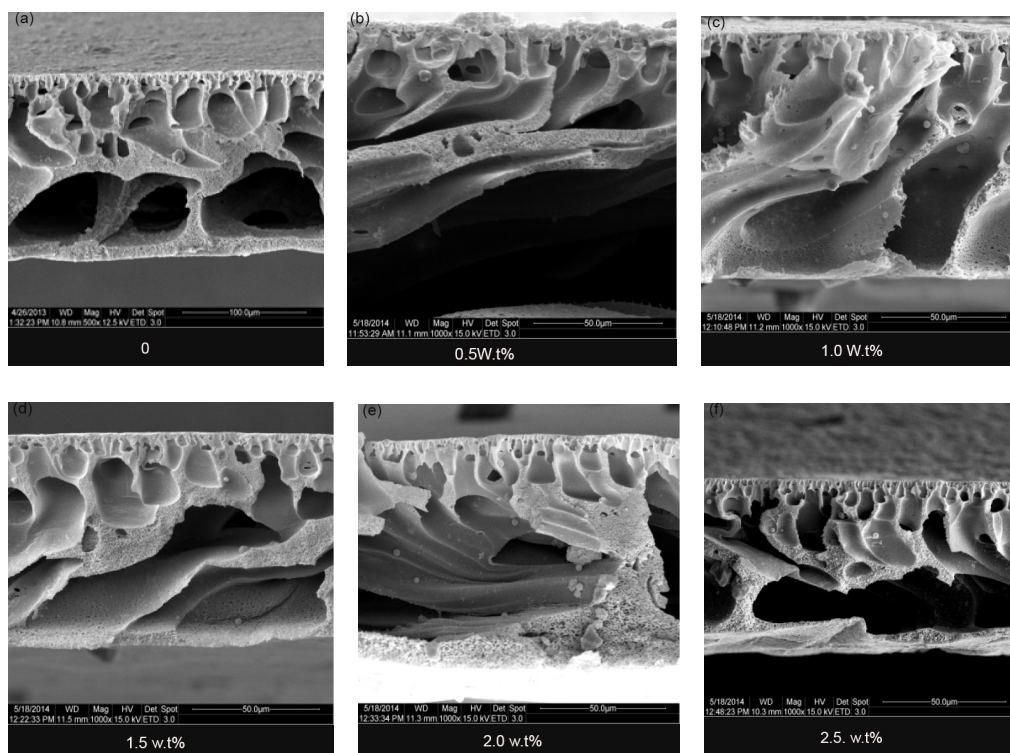
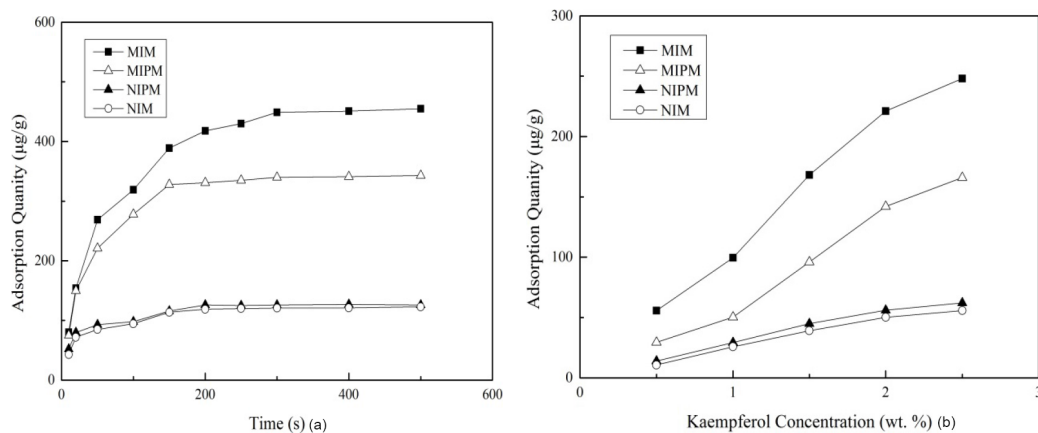Fig. 10. Cross-sectional SEM micro graphs of membranes for different imprinted polymer sphere concentrations.

Fig. 11. Adsorption kinetic curve (a) and adsorption isotherm(b) of molecular imprinting membranes.

Table 4
The equilibrium dissociation constant (KD) and separation factor (α) of molecular imprinting membranes

Substrate	$K_{D\ kaempferol}$ ml/g	$K_{D\ rutin}$ ml/g	α
MIM	48.42	12.91	3.75
MIPM	38.39	11.13	3.45
NIPM	18.56	16.47	1.13
NIM	13.43	14.11	0.95

MIM, molecularly imprinted membranes; MIPM, molecularly imprinted polymer membrane; NIPM, non-molecularly imprinted polymer membrane; NIM, non-molecularly imprinted membrane.

References

[1] Z.J. Huang, P. Zhang, Y.B. Yun, Preparing molecularly imprinted membranes by phase inversion to separate kaempferol, Polym. Adv. Technol., 3 (2017) 28.
[2] V. Kochkodan, W. Weigel, M. Ulbricht, Molecularly imprinted composite membranes for selective binding of desmetryn from aqueous solutions, Desalination, 149 (2002) 323–328.

[3] C. Chen, Y. Chen, J. Zhou, C. Wu, A 9-vinyladenine-based molecularly imprinted polymeric membrane for the efficient recognition of plant hormone 1 H-indole-3-acetic acid, Anal. Chim. Acta, 569 (2006) 58–65.

[4] P. Qin, C. Chen, B. Han, S. Takuji, J. Li, B. Sun, Preparation of poly(phthalazinone ether sulfone ketone) asymmetric ultra filtration membrane : II. The gelation process, J. Membr. Sci., 268 (2006) 181–188.

[5] M. Ulbricht, Membrane separations using molecularly imprinted polymers, J. Chromatogr. B., 804 (2004) 113.

[6] G. Wulff, Molecular imprinting in cross-linked materials with the aid of molecular templates-a way toward artificial antibodies, Angew. Chem. Int. Ed. Engl., 34 (1995) 1812.

[7] M. Lehmann, H. Brunner, G. Tovar, Molecularly imprinted nano particles as selective phase in composite membranes-hydrodynamics and separation in nano scale beds, Chem. Ing. Tech., 75 (2003) 149–153.

[8] C. Borrelli, S. Barsanti, D. Silvestri, P. Manesiotis, G. Ciardelli, B. Sellergren, Selective depletion of riboflavine from beer using membranes incorporating imprinted polymer particles, J. Food Process. Pres., 35 (2011) 112–128.

[9] L. Donato, F. Tasselli, G. De Luca, S. Garcia Del Blanco, E. Drioli, Novel hybrid molecularly imprinted membranes for targeted 4,4-methylendianiline, Sep. Purif. Technol., 116 (2013) 184–191.

[10] I.I. Nasser, C. Algieri, A. Garofalo, E. Drioli, C. Ahmed, L. Donato, Hybrid imprinted membranes for selective recognition of quercetin, Sep. Purif. Technol., 163 (2016) 331–340.

[11] W. Hong, Z. Yanyan, N. Mingcheng, J. Zhongyi, Molecularly imprinted organic–inorganic hybrid membranes for selective separation of phenylalanine isomers and its analogue, Sep. Purif. Technol., 68 (2009) 97–104.

[12] R. Malaisamy, M. Ulbricht, Evaluation of molecularly imprinted polymer blend filtration membranes under solid phase extraction conditions, Sep. Purif. Methods, 39 (2004) 211–219.

[13] P. Fan, B. Wang, Preparation of molecularly imprinted polymer membrane with blending trimethoprim-MIP and polysulfone and its transport properties, Korean J. Chem. Eng., 26 (2009) 1813–1820.

[14] E. Saljoughi, M. Amirilargani, T. Mohammadi, Asymmetric cellulose acetate dialysis membranes: Synthesis, characterization, and performance, J. Appl. Polym. Sci., 116 (2010) 2251–2259.

[15] E. Fontananova, J.C. Jansen, A. Cristiano, E. Curcio, E. Drioli, Effect of additives in the casting solution on the formation of PVDF membranes, Desalination, 192 (2006) 190–197.

[16] I.C. Kim, K.H. Lee, Effect of various additives on pore size of polysulfone membrane by phase-inversion process, J. Appl. Polym. Sci., 89 (2003) 2562–2566.

[17] X. Li, C. Chen, J. Li, Y. Su, Effect of ethylene glycol monobutyl ether on skin layer formation kinetics of asymmetric membranes, J. Appl. Polym. Sci., 113 (2010) 2392–2396.

[18] L. Zheng, Effect of salt additive on the formation of micro porous poly(vinylidene fluoride) membranes by phase inversion from $LiClO_4$/Water/DMF/PVDF system, Polym., 44 (2003) 413–422.

[19] X. Li, C. Chen, J. Li, Erratum to "Formation kinetics of polyethersulfone with cardo membrane via phase inversion" [J. Membr. Sci., 314 (2008) 206–211], J. Membr. Sci., 340 (2008) 272–274.

[20] L.P. Cheng, T.H. Young, L. Fang, J.J. Gau, Formation of particulate micro porous poly (vinylidene fluoride) membranes by isothermal immersion precipitation from the 1-octanol/dimethylformamide/poly(vinylidene fluoride) system, Polym., 40 (1999) 2395–2403.

[21] M.C. Yang, W.C. Lin, Surface modification and blood compatibility of polyacrylonitrile membrane with immobilized chitosan–heparin conjugate, J. Polym. Res., 9 (2002) 201–206.

[22] K. Nouzaki, M. Nagata, J. Arai, Y. Idemoto, N. Koura, H. Yanagishita, H. Negishi, D. Kitamoto, T. Ikegami, K. Haraya, Preparation of polyacrylonitrile ultra filtration membranes for wastewater treatment , Desalination, 144 (2002) 53–59.

[23] E. Yuliwati, A.F. Ismail, Effect of additives concentration on the surface properties and performance of PVDF ultra filtration membranes for refinery produced wastewater treatment, Desalination, 273 (2011) 226–234.